Available online at www.sciencedirect.com
ScienceDirect
Journal of the European Ceramic Society 28 (2008) 2709–2716
www.elsevier.com/locate/jeurceramsoc

Effects of dopant concentration and calcination temperature on the microstructure of Ca-doped ceria nanopowders

M. Yan [a,*], T. Mori [a], F. Ye [a], D.R. Ou [a], J. Zou [b,c], J. Drennan [c]

[a] *Fuel Cell Materials Center, National Institute for Materials Science, 1-1 Namiki, Tsukuba, Ibaraki 305-0044, Japan*
[b] *School of Engineering, The University of Queensland, Brisbane, QLD 4072, Australia*
[c] *Centre for Microscopy and Microanalysis, The University of Queensland, Brisbane, QLD 4072, Australia*

Received 18 March 2008; received in revised form 22 April 2008; accepted 22 April 2008
Available online 3 June 2008

Abstract

We demonstrate a systematic investigation on the microstructure of the Ca-doped ceria affected by different dopant concentrations and calcination temperatures. It has been shown that nanopowders of Ca-doped ceria have been successfully prepared in a broad dopant concentration region from 5 at.% to 70 at.%. By using various microstructure analysis techniques, the secondary phase has been determined, and the solubility of Ca in ceria has been realized to be less than 20 at.%. It has been also found that the calcination temperature greatly affects the grain growth of the calcined powders, and high temperature calcination treatments would cause lattice relaxation and lead to precipitations, based on which proper calcination conditions are suggested.

Keywords: Powders-chemical preparation; Electron microscopy; Microstructure-final; CeO_2; Fuel cells

1. Introduction

Aliovalent elements doped ceria have been studied extensively as electrolyte materials for solid oxide fuel cells (SOFCs) because of their high ionic conductivity at the intermediate temperature region (300–500 °C). Particularly, the trivalent rare earth elements (e.g. Sm and Gd) doped ceria have been pursued for their relatively better transport properties.[1–3] However, it is well known that mining and extracting the rare earth elements from minerals are difficult and, accordingly, an intense environmental burden will be induced if they are heavily utilized. In contrast, because of its abundance in the planet, the divalent element, Ca, could be the competitive candidate for the commercialization of SOFCs from the environmentally friendly reason and its comparatively cheaper price, particular if the conductivity of the electrolyte made by Ca-doped ceria could be improved to a level comparable to the rare earth elements doped ceria.

Although the study of Ca-doped ceria was started as early as 1970s,[4,5] the focus in the previous studies was mainly on the ionic conductivity performance.[4–9] As a consequence, microstructure studies on the Ca-doped ceria were fairly limited,[10–12] and detailed microstructural characteristics remain unclear though such information is critical for the design and manufacture of SOFCs based on Ca-doped ceria.

In this study, two important factors, i.e. the dopant concentration and the calcination temperature, were systematically investigated in terms of their effects on the microstructure of the Ca-doped ceria nanopowders.

2. Experimental

2.1. Powder preparation

Precursor powders with the compositions of $Ca_xCe_{1-x}O_{2-y}$ ($x = 0.05, 0.1, 0.2, 0.3, 0.4, 0.5, 0.6$, and 0.7) were prepared by a co-precipitation method. High purity (>99.99%) cerium nitrate hexhydrate ($Ce(NO_3)_3{\cdot}6H_2O$), calcium nitrate tetrahydrate ($Ca(NO_3)_2{\cdot}4H_2O$) and ammonium carbonate ($(NH_4)_2CO_3$) were used for the powder preparation. The precipitation temperature was kept at 40–50 °C and the ratio between the cations and the carbonate was 4–6, both of which depend upon the dopant concentration. Fine powders with the dopant concentra-

* Corresponding author.
E-mail address: YAN.Ming@nims.go.jp (M. Yan).

0955-2219/$ – see front matter © 2008 Elsevier Ltd. All rights reserved.
doi:10.1016/j.jeurceramsoc.2008.04.016

tion beyond 70 at.% were extremely difficult to obtain by using the above pathways and, accordingly, their microstructures were not investigated in this study. Raw powders were washed firstly by distilled water and then by ethanol for at least three times, and they were subsequently dried under the nitrogen gas flow for 24 h. Dried powders were pulverized and sieved to be ready for the analysis as precursor powders. Since it is suggested theoretically and experimentally that the calcination temperature has more evident impacts on the resultant microstructures of the calcined powders than the holding time,[13–15] the calcination treatment was performed at different temperatures (550 °C, 700 °C, 850 °C and 1000 °C) and the holding time was fixed at 2 h, which duration was proved to be sufficient for the doped ceria materials.[16] The heating rate of the calcination treatment was controlled at 5 °C/min and the calcined powders were cooled to the room temperature within the furnace. Powders dispersed by ethanol or powder compacts (to provide a flat surface for the microstructure analysis) made by a rubber press (∼15 MPa) were used in the microstructure studies.

2.2. Microstructure characterization

Microstructures of the obtained powders were investigated by scanning electron microscopy (SEM, Hitachi S-5000, 10 keV/10 mA; Hitachi S-5800, 20 keV/10 mA), transmission electron microscopy (TEM, JEOL NM-200, 200 kV), differential thermal analysis/thermogravimetry (DTA/TG, SEIKO EXSTRASR6200) and X-ray diffractometer (XRD, Rigaku RINT 2000HF Ultima, 40 kV/40 mA). DTA was performed in air at a pressure of 1 atm with a heating rate of 10 °C/min, using a platinum crucible as the sample container, and the obtained results had a temperature accuracy of ±2 K. XRD was performed at a scanning rate of 2° min^{-1} by using a Cu Kα radiation, and the XRD patterns were utilized to determine the lattice parameter of the corresponding powders by using an extrapolation method,[17] which error was determined within ±0.0001 nm. The averaged grain size of the powders was determined based on the SEM observations of more than 30 particles for each sample.

3. Results

3.1. Characterization of Ca-doped ceria nanopowders

Fig. 1(a)–(c) shows the SEM secondary electron (SEM-SE) images for the precursor powders with 10 at.% Ca (abbreviated as 10Ca, similarly hereafter), 40Ca and 70Ca doped ceria, respectively. As can be seen, nano-sized powders have been successfully achieved. Extensive SEM investigations suggested that all the precursor powders have their averaged particle size in a narrow range of 27–37 nm (see Table 1 for details). In addition, varying the dopant concentration does not affect the shape or particle size of the precursor powders.

Fig. 2 presents the XRD patterns for the precursor powders and shows that the precursor powders generally have a very low crystallity, which is a common feature for the chemical-route prepared powders because of the absorbed molecular waters,[16,18] and this structural feature dominates in the dopant concentration region between 5Ca and 60Ca; beyond which, evidences of crystalline phases can be seen.

Fig. 3 shows the differential TG results for the precursor powders that were obtained from the DTA/TG experiments. As can be seen from this figure, two major weight loss processes (corresponding to the temperatures of 70–250 °C and 250–500 °C) are recorded for the 5Ca and 10Ca powders, which might correspond to a step of releasing the absorbed moisture and the molecular water and to a step of Ce-based carbonates' decomposition.[16] For higher Ca-doped (≥20Ca) powders, however, an additional weight loss peak can be recognized, suggesting that additional

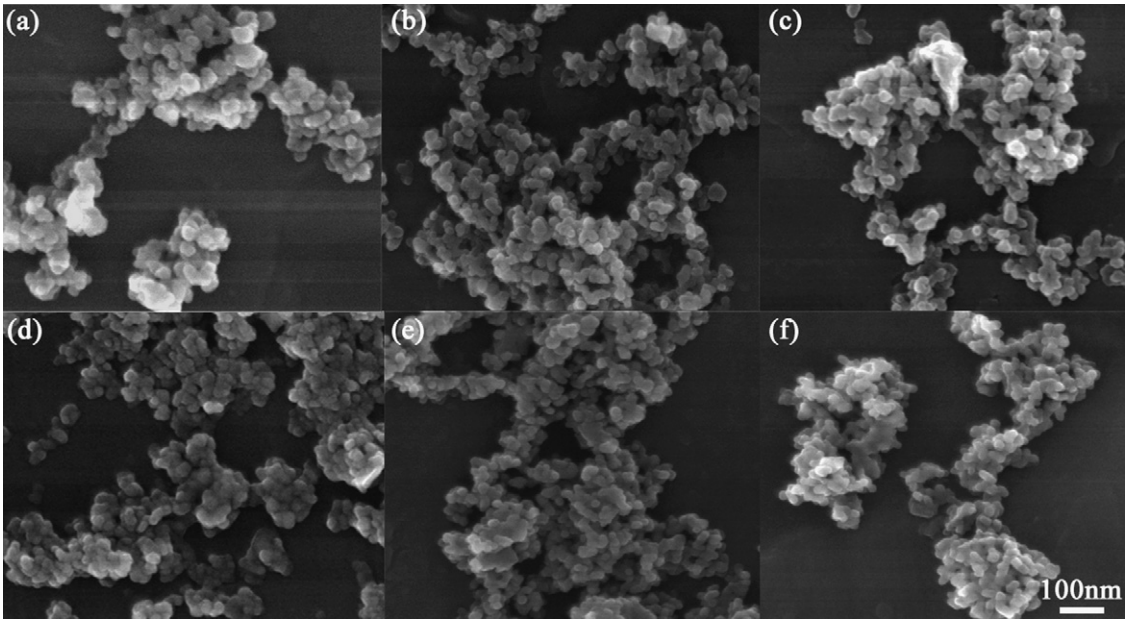

Fig. 1. SEM-SE images for the powders: (a) 10Ca precursor, (b) 40Ca precursor, (c) 70Ca precursor, (d) 10Ca-700, (e) 40Ca-700 and (f) 70Ca-700.

Table 1
Averaged grain size of the powders determined by the SEM observations

	Sample							
	5Ca	10Ca	20Ca	30Ca	40Ca	50Ca	60Ca	70Ca
d (nm)	34	37	31	27	29	32	33	31
	Sample							
	5Ca-700	10Ca-700	20Ca-700	30Ca-700	40Ca-700	50Ca-700	60Ca-700	70Ca-700
d (nm)	35	34	27	25	26	29	27	27
	Sample							
	70Ca-550		70Ca-700		70Ca-850		70Ca-1000	
d (nm)	24		27		64		137	

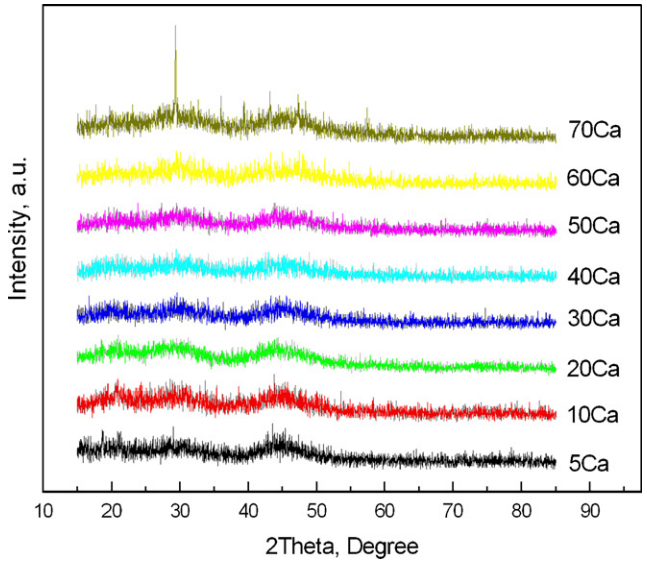

Fig. 2. XRD patterns for the precursor powders.

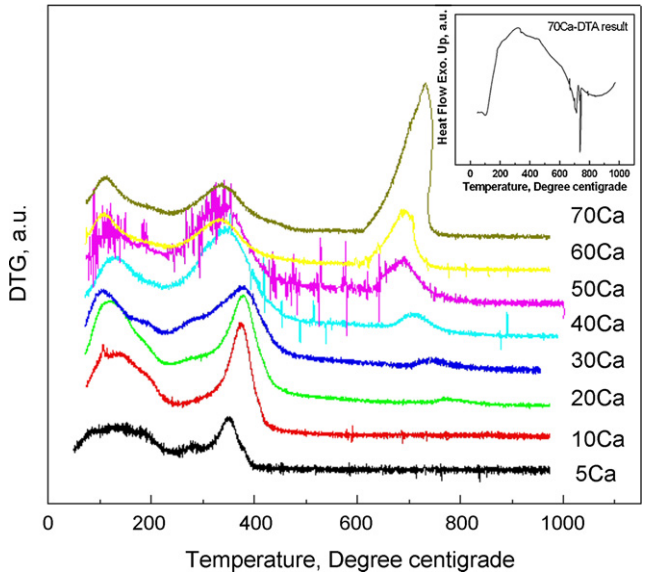

Fig. 3. Differential TG results showing the weight loss process for the precursor powders. Figure inset is the DTA result for the 70Ca powder.

phases besides the doped ceria might form during the powder preparation process when the dopant concentration is equal or higher than 20 at.%. Since this peak becomes stronger with increasing the Ca concentration, we anticipate that this peak should be related to a decomposition process of Ca-based complexes. At the same time, it is noticed that the temperature of the additional peak shows a tendency of decreasing with the increasing dopant concentration, suggesting that the composition of the aforementioned Ca-based complexes might be firstly close to $CaCO_3$ (889 °C as its standard decomposition temperature)[19] in the cases of lower dopant concentrations then be composed of both the $CaCO_3$ and the $Ca(OH)_2$ (512 °C as its standard decomposition temperature)[20] in the cases of higher dopant concentrations. It should be also noted that there seems to be a back-shift of the peak position in the 70Ca powder. However, the temperature center of this peak still agrees with the above regulation and it is anticipated that the disturbed heat conduction process (see the inset for the DTA record of this powder) contributed to this asymmetrical peak, which was proved to be vanished in normal situations by repeated experiments.

3.2. Dopant concentration effects on the microstructure

To understand the effects of the dopant concentration on the microstructure of the calcined powders, we systematically investigated the powders calcined at 700 °C for 2 h. Fig. 1(d)–(f) are typical SEM images of the calcined powders with their compositions being 10Ca, 40Ca and 70Ca, respectively. The comparison of these three images indicates that the morphology of the calcined powders was not affected by the increasing dopant concentration and their sizes are distributed in the region of 25–35 nm (see Table 1 for details).

Fig. 4 provides the XRD patterns of the calcined powders and indicates that the main structure is fluorite, while traces of the secondary phase start to be recognized from 50Ca powders calcined at 700 °C (abbreviated as 50Ca-700, similarly hereafter) and there is a tendency of the higher the dopant concentration, the stronger the diffraction peaks of the secondary phase. Moreover, Fig. 5 presents a typical element mapping analysis for the secondary phase (with darker contrast) from the 70Ca-700 powder compact, which indicates that Ca and O are enriched

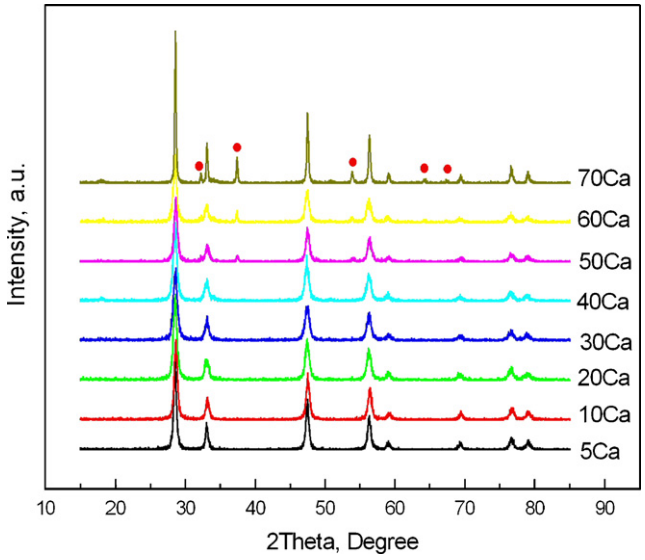

Fig. 4. XRD patterns for the 700 °C calcined powders. Diffractions except those for the doped ceria are marked out by spots for 70Ca-700.

in its composition and Ce is less contained comparatively. By checking the corresponding XRD results and combining them with the compositional information, the secondary phase can be determined to be a CaO-based solid solution containing a small amount of cerium, which crystal structure is very close to the standard FCC structured CaO with a lattice parameter of $a_{CaO} = 0.480$ nm and a space group of Fm3m (PDF 82-1691).

To further clarify this point, TEM was employed. In order to accurately determine the diffraction spots and, in turn, to determine the crystal phase(s), Au was coated on top of the specimen for calibrating the camera length as the lattice parameter of Au ($a_{Au} = 0.406$ nm) is known. Fig. 6 shows the selected area electron diffraction (SAED) patterns [Fig. 6(a) and (b)] and the corresponding bright-field images [Fig. 6(c) and (d)] for the secondary phase and the 70Ca-700 powder. Since Au has an FCC structure and coated Au has a form of polycrystalline, the first diffraction ring must be from its $\langle 1\,1\,1\rangle^*$ and corresponds to the lattice spacing of $d_{1\,1\,1(Au)} = 0.235$ nm. As can be seen from Fig. 6(a), the lattice spacing of a diffraction spot, marked by a line and very close to $\langle 1\,1\,1\rangle^*_{Au}$, can be determined to be 0.24 nm, which corresponds to be $\langle 0\,0\,2\rangle^*_{CaO}$; while, similarly, the lattice spacing of a diffraction spot near $\langle 1\,1\,1\rangle^*_{Au}$ can be determined to be the $\langle 0\,0\,2\rangle^*$ of the doped ceria as shown in Fig. 6(b).

Although the solubility of Ca in ceria was previously suggested to be about 23 at.%,[10,11] it is noted that those results mainly came from the XRD measurements rather than direct observations. At the same time, it is known that XRD is limited in its sensitivity and affected by the machine power. Consequently, SEM back scattered electron (SEM-BSE) images were recorded in order to specify this point and selective results are shown in Fig. 7. Fig. 7(a) is an SEM-BSE image of the 10Ca-700 powder compact and shows the morphology is almost contrastless, suggesting that the structure is dominated by the fluorite doped ceria; although the secondary phase can be observed very occa-

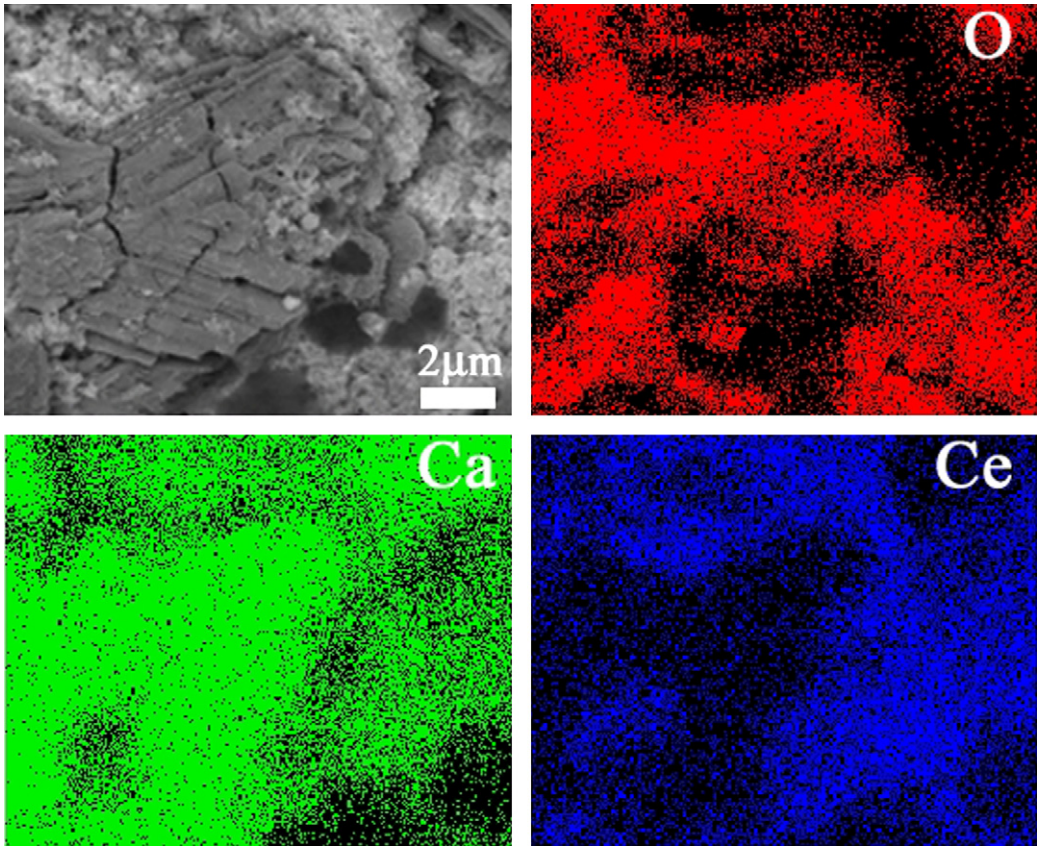

Fig. 5. SEM-EDX element mapping results showing the distribution of O, Ca and Ce in the 70Ca-700 powder compact.

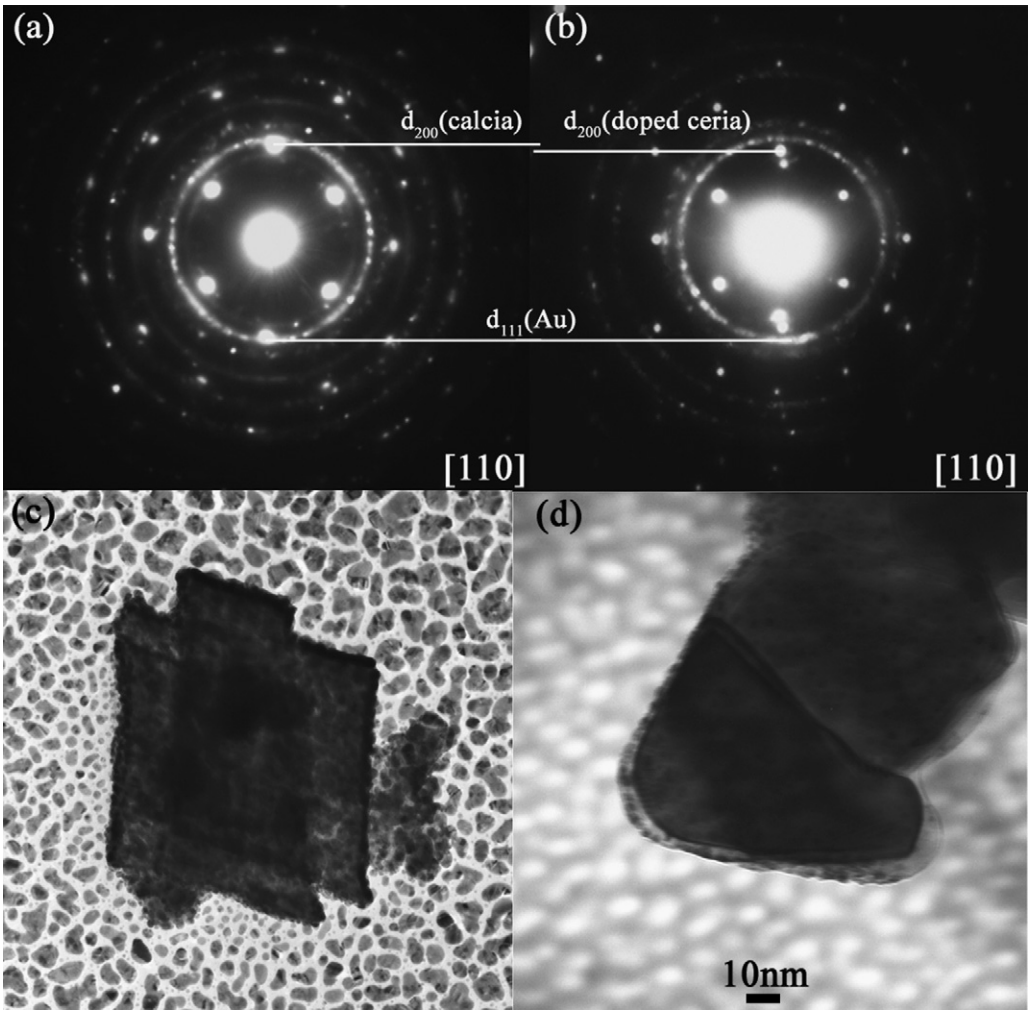

Fig. 6. TEM results for the 70Ca-700 powders: (a) SAED patterns for calcia, (b) SAED patterns for doped ceria, (c) bright-field image for calcia and (d) bright-field image for doped ceria.

sionally, as shown by the inset. In contrast, the secondary phase can be frequently observed in the 20Ca-700 powder compact [Fig. 7(b)], which becomes a remarkable feature in the 70Ca-700 [Fig. 7(c)]. And the reason for that the XRD result for the 20Ca-700 powder in Fig. 4 does not clearly show the corresponding diffractions of the secondary phase should be due to its low amount in this composition, which is beyond the sensitivity of XRD. Based on these, we anticipate that the solubility of Ca in ceria should be below 20 at.% for the calcined powders. In fact, our study of the sintered Ca-doped ceria materials also proved this judgment, and the details of the relevant results will be present elsewhere.

3.3. Calcination temperature effects on the microstructure

To investigate the calcination temperature effects on the microstructure, calcination treatments at four different temperatures (550 °C, 700 °C, 850 °C and 1000 °C) were conducted for

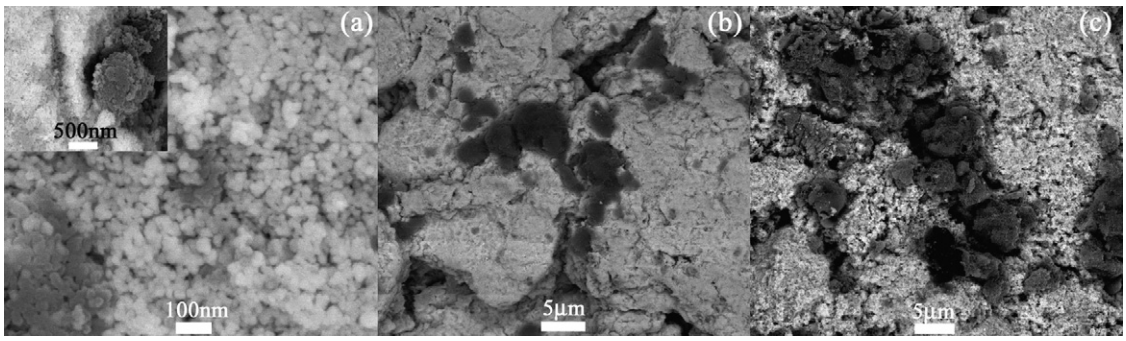

Fig. 7. SEM-BSE images for the 700 °C calcined powder compacts: (a) 10Ca, (b) 20Ca and (c) 70Ca. Inset picture in (a) shows an image for the secondary phase.

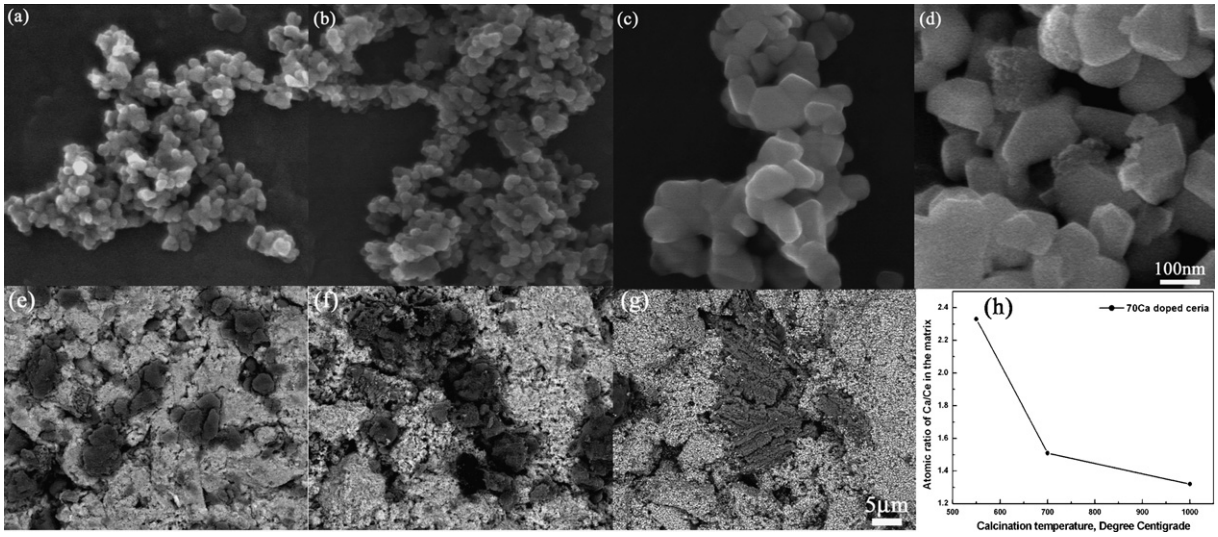

Fig. 8. SEM-SE images for (a) 70Ca-550, (b) 70Ca-700, (c) 70Ca-850, (d) 70Ca-1000, and SEM-BSE images for (e) 70Ca-550, (f) 70Ca-700, (g) 70Ca-1000 powder compact. The corresponding SEM-EDX results for these calcined powders are shown in (h).

the precursor powders and the resultant microstructures were investigated.

As typical examples, Fig. 8(a)–(d) shows SEM-SE images of the 70Ca powders calcined at 550 °C, 700 °C, 850 °C and 1000 °C, respectively. As can be seen, calcination temperature greatly affects the morphology of the calcined powders, which causes about six times grain growth from the calcination at 550 °C to 1000 °C (Table 1). Fig. 8(e)–(g) are the

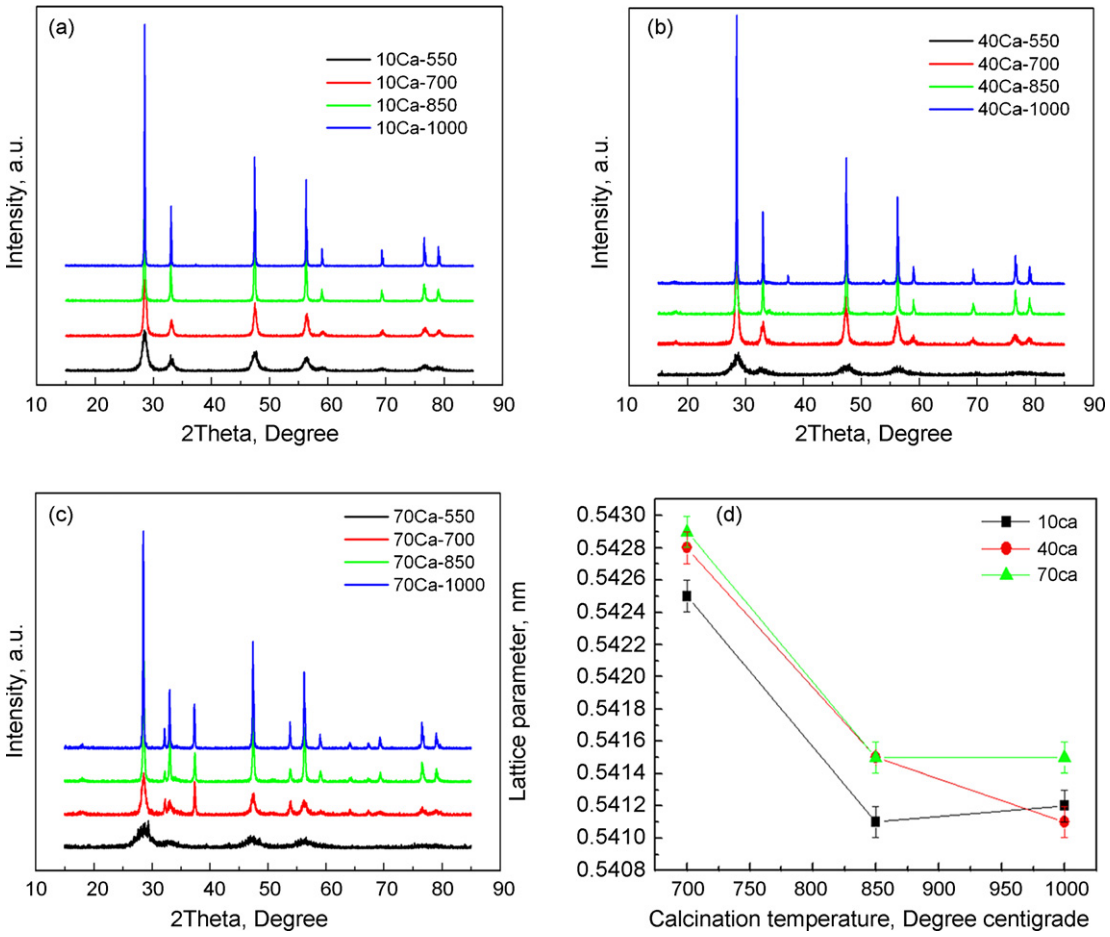

Fig. 9. XRD patterns for the (a) 10Ca, (b) 40Ca and (c) 70Ca powders that are calcined at different temperatures. The corresponding lattice parameter as a function of the calcination temperature is shown in (d). Error bars are also given in this figure.

SEM-BSE images of the 70Ca powders calcined at 550 °C, 700 °C and 1000 °C, respectively. Comparison of these SEM-BSE images indicates that higher calcination temperature causes higher degree of aggregation of the secondary phases, and this tendency also applies to other compositions. A supporting point to this observation is that the ratio of Ca/Ce in the matrix (which is composed of the dispersed secondary phase and the doped ceria) is decreased as the calcination temperature increases (see Fig. 8(h) for the details). Since Ca is expected to be enriched in the secondary phase, this suggests a less amount of dispersed secondary phases in the matrix and, in turn, confirms that a higher degree of aggregation of the secondary phase is introduced by the higher temperature calcinations.

Fig. 9(a)–(c) presents the XRD patterns for the 10Ca, 40Ca and 70Ca powders calcined at those four temperatures. By analyzing the relevant diffraction results (except those from 550 °C calcination which diffraction peaks are too broad and subject to large errors), the lattice parameter of the calcined powders as a function of the calcination temperature can be obtained and the results are shown in Fig. 9(d). Based on this, a general trend can be concluded that the lattice parameter of the doped ceria decreases with the increasing calcination temperature from 700 °C to 850 °C, while the difference in the lattice parameter between the 850 °C and 1000 °C calcinations becomes very small, suggesting two likely scenarios: (1) a high temperature calcination might decrease the lattice parameter through forming Ca-enriched precipitations since, from the Vegard's law, the concentration of the solute (Ca in the current case) determines the lattice parameters of the solution (doped ceria) and (2) the 850 °C calcination might have already achieved the maximum effects on the lattice parameter and calcinations at higher temperatures than it will not show obvious difference in the results.

4. Discussion

Among the aforementioned results, the first issue to note is that, in the broad dopant concentration region from 5 at.% to 70 at.%, well-dispersed round shaped nanopowders have been successfully prepared. Although using chemical routes to prepare the Ca-doped ceria powders were reported previously,[12] it is the first demonstration that nanopowders can be prepared in such a wide Ca concentration region. This, in turn, provides more opportunities to study the behavior of heavily Ca-doped ceria nanopowders.

In terms of the secondary phase, various techniques have been used to obtain a proper and a comprehensive understanding. Since the secondary phase has been found in the 20Ca, the solubility of Ca in ceria is realized to be less than 20 at.%, which is suggested to be around 10 at.% by recalling the SEM-BSE images shown in Fig. 7. At the same time, since a solid solution with the crystal structure identical to FCC CaO is determined to be the secondary phase and since CaO is believed to be an isolating phase to the ionic conduction,[10] the appropriate doping level of Ca to ceria should be around 10 at.%, based on the fact that the extra isolating phases would affect the bulk ionic conductivity negatively.

It has been noted that the calcination temperature has great effects on the morphology and structure of the calcined powders. It is understandable that higher temperature calcination leads to larger powder size, since the calcination treatment is basically a decomposition process together with a heat-activated grain growth procedure. In addition, the phenomenon that high temperature calcination treatments decrease the lattice parameter is noticeable. On this point, we suggest a following scenario: since the ionic radius of Ce^{4+} is about 0.097 nm and, for Ca^{2+}, this value is about 0.112 nm,[11,21] when the larger Ca^{2+} cations substitute the smaller Ce^{4+} cations to form oxygen vacancies, a lattice distortion must be introduced because of the mismatch between different radii. In this case, if the calcination temperature is increased, a higher energy will be provided to the system and some of the lattice distortion could be accommodated by forming local precipitations. To support this point, Fig. 10 presents the TEM bright-field [Fig. 10(a)] and dark-field [Fig. 10(b)] images for the 10Ca-1000 powders. As can be seen, extra contrasts could be observed in the bright-field image and, especially, the dark-field image, confirming precipitations have

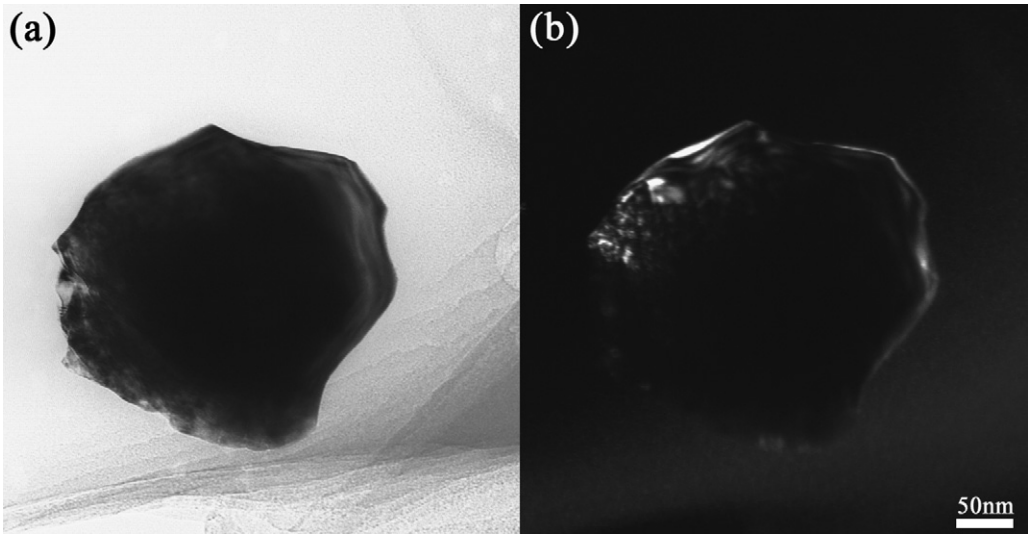

Fig. 10. TEM results for the 10Ca-1000 powders: (a) a bright-field image and (b) a dark-field image.

taken place. At the same time, it is known that, in the field of ionic conducting materials, these kinds of precipitations are generally considered to be microdomains,[22,23] which might contain a higher amount of dopant cations and have certain degree of crystallity. As such, since it has been demonstrated that usually microdomains would have negative effects on the bulk conductivity of the doped ceria materials,[24–27] cautions must be paid when designing the calcination pathways for the Ca-doped ceria materials.

5. Conclusions

Through a systematic study on the microstructure of the Ca-doped ceria nanopowders in a large dopant concentration region, following conclusions can be made:

(1) Ca-doped ceria nanopowders have been successfully fabricated in a wide calcium concentration region from 5 at.% to 70 at.%. This consequently provides the opportunities for studies in the heavily Ca-doped ceria materials.
(2) When the calcium concentration is higher than (or equal to) 20 at.%, the system will become a mixture of the doped ceria and the secondary phase; and the secondary phase itself is determined to be a solid solution enriched in Ca and O together with a small amount of Ce, which crystal structure is very close to the FCC CaO ($a = 0.480$ nm, PDF 82-1691).
(3) Calcination temperature shows great effects on the morphology of the calcined powders. When the calcination temperature is high (e.g. 850 °C), the lattice parameter of the doped ceria will be decreased and local precipitations are introduced.

References

1. Balazs, G. B. and Glass, R. S., *Solid Sate Ionics*, 1995, **76**, 155.
2. Yahiro, H., Eguchi, K. and Arai, H., *Solid State Ionics*, 1989, **36**, 71.
3. Arai, H., Kunisaki, T., Shimizu, Y. and Seiyama, T., *Solid State Ionics*, 1986, **20**, 241.
4. Blumenthal, R. N., Brugner, F. S. and Garnier, J. E., *J. Electrochem. Soc.*, 1973, **120**, 1230.
5. Tuller, H. L. and Nowick, A. S., *J. Electrochem. Soc.*, 1975, **122**, 255.
6. Wang, D. Y. and Nowick, A. S., *J. Solid State Chem.*, 1980, **35**, 325.
7. El Adham, K. and Hammou, A., *Solid State Ionics*, 1983, **9**(10), 905.
8. Zhu, B., Liu, X. R., Sun, M. T., Ji, S. J. and Sun, J. C., *Solid State Sci.*, 2003, **5**, 1127.
9. Lu, Z., Huang, X. Q., Liu, W., He, T. M., Liu, Z. G., Liu, J. and Su, W. H., *J. Rare Earths*, 2002, **20**, 47.
10. Eguchi, K., Kunisaki, T. and Arai, H., *J. Am. Ceram. Soc.*, 1986, **69**, C282.
11. Yahiro, H., Ohuchi, T., Eguchi, K. and Arai, H., *J. Mater. Sci.*, 1988, **23**, 1036.
12. Thangadurai, V. and Kopp, P., *J. Power Sources*, 2007, **168**, 178.
13. Klingsbrg, C., *The Physics and Chemistry of Ceramics*. Gordonnn & Breach, 1963, pp. 165–179.
14. Kingery, W. D., Bowen, H. K. and Uhlmann, D. R., *Introduction to Ceramics* (*2nd ed.*). John Wiley & Sons, 1976, pp. 449–516.
15. Huang, J. B., Mao, Z. Q., Yang, L. Z. and Peng, R. R., *Electrochem. Solid-State Lett.*, 2005, **8**, A437.
16. Wang, Y. R., Mori, T., Li, J. G., Ikegami, T. and Yajima, Y., *J. Mater. Res.*, 2003, **18**, 1239.
17. Brown, J. G., *X-Ray and Their Applications*. London Iliffe Books, 1966, pp. 203–237.
18. Li, J. G., Ikegami, T. and Mori, T., *Acta Mater.*, 2004, **52**, 2221.
19. International Chemical Safety Card 1193.
20. Halstead, P. E. and Moore, A. E., *J. Chem. Soc. Sep.*, 1957, 3873.
21. Inaba, H. and Tagawa, H., *Solid State Ionics*, 1996, **83**, 1.
22. Drennan, J. and Auchterlonie, G., *Solid State Ionics*, 2000, **134**, 75.
23. Rossell, H. J., Sellar, J. R. and Wilson, I. J., *Acta Crystallogr.*, 1991, **47**, B862.
24. Ye, F., Mori, T., Ou, D. R., Takahashi, M., Zou, J. and Drennan, J., *J. Electrochem. Soc.*, 2007, **154**, B180.
25. Ou, D. R., Mori, T., Ye, F., Zou, J., Auchterlonie, G. and Drennan, J., *Electrochem. Solid-State Lett.*, 2007, **10**, 1.
26. Mori, T., Wang, Y. R., Drennan, J., Auchterlonie, G., Li, J. G. and Ikegami, T., *Solid State Ionics*, 2004, **175**, 641.
27. Mori, T., Drennan, J., Wang, Y. R., Auchterlonie, G., Li, J. G. and Yago, A., *Sci. Tech. Adv. Mater.*, 2003, **4**, 213.